Inorganic Chemistry
Article
Cite This: Inorg. Chem. XXXX, XXX, XXX−XXX
pubs.acs.org/IC

Highly Active Ruthenium CNC Pincer Photocatalysts for Visible-Light-Driven Carbon Dioxide Reduction

Sanjit Das,[†,#] Roberta R. Rodrigues,[‡,#] Robert W. Lamb,[§] Fengrui Qu,[†] Eric Reinheimer,[∥] Chance M. Boudreaux,[†] Charles Edwin Webster,*[,§] Jared H. Delcamp,*[,‡] and Elizabeth T. Papish*[,†]

[†]Department of Chemistry and Biochemistry, University of Alabama, Shelby Hall, Tuscaloosa, Alabama 35487, United States
[‡]Department of Chemistry and Biochemistry, University of Mississippi, Coulter Hall, Oxford, Mississippi 38677, United States
[§]Department of Chemistry, Mississippi State University, Mississippi State, Mississippi 39762, United States
[∥]Rigaku Oxford Diffraction, 9009 New Trails Drive, The Woodlands, Texas 77381, United States

Supporting Information

ABSTRACT: Five ruthenium catalysts described herein facilitate self-sensitized carbon dioxide reduction to form carbon monoxide with a ruthenium catalytic center. These catalysts include four new and one previously reported CNC pincer complexes featuring a pyridinol derived *N*-donor and *N*-heterocyclic carbene (NHC) C-donors derived from imidazole or benzimidazole. The complexes have been characterized fully by spectroscopic and analytic methods, including X-ray crystallography. Introduction of a 2,2′-bipyridine (bipy) coligand and phenyl groups on the NHC ligand was necessary for rapid catalysis. $[(CNC)Ru(bipy)(CH_3CN)](OTf)_2$ is among the most active and durable photocatalysts in the literature for CO_2 reduction without an external photosensitizer. The role of the structure of this complex in catalysis is discussed, including the importance of the pincer's phenyl wingtips, the bipyridyl ligand, and a weakly coordinating monodentate ligand.

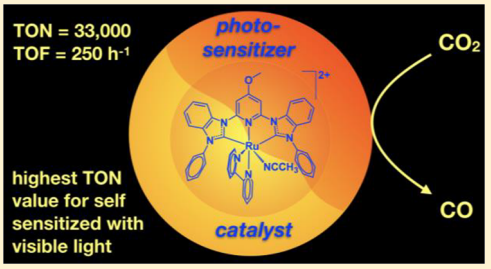

INTRODUCTION

The efficient and selective photocatalytic conversion of carbon dioxide to a usable fuel remains a grand challenge.[1−4] The addition of an oxygen-bearing group to CNC pincer ligands (Chart 1) has been transformative for both ruthenium- and nickel-catalyzed carbon dioxide reduction.[5,6] We previously reported ruthenium(II) (**4**)[5,7] and nickel(II) (**5**)[6] complexes that catalyze CO_2 reduction in the presence of a photosensitizer (PS, e.g., $Ir(ppy)_3$ where ppy = 2-phenylpyridine) and sacrificial donors (SDs: triethylamine (TEA) and 1,3-dimethyl-2-phenyl-2,3-dihydro-1*H*-benzo[*d*]imidazole (BIH)). Catalyst (**4**) selectively generates CO for 40 h (turnover number (TON) = 250), whereas the unsubstituted analog, with H in place of the methoxy group, is inactive.[5] The oxygen-bearing groups in both **4** and **5** lower the redox potentials such that the thermodynamics are favorable for both electron transfer from the PS to the catalyst and from the catalyst to CO_2 at the first reduction potential.[5,6] Thus, visible light is able to provide the driving force for these reactions. However, one drawback is that a precious metal photosensitizer (PS, e.g. $Ir(ppy)_3$) is needed for light-harvesting. In this work, we demonstrate that with a change to the ligand scaffold CO_2 reduction without an additional PS is feasible and can produce quantities of CO comparable to the sensitized reactions. Such self-sensitized visible-light-driven CO_2 reduction reactions using mononuclear catalysts have been rare in the literature with limited ligand scaffolds featuring Ir, Re, Ru, and Fe

Chart 1. Self-Sensitized (1−3) and Prior-Photosensitized (4 and 5) Complexes Tested for Light-Driven CO_2 Reduction[a]

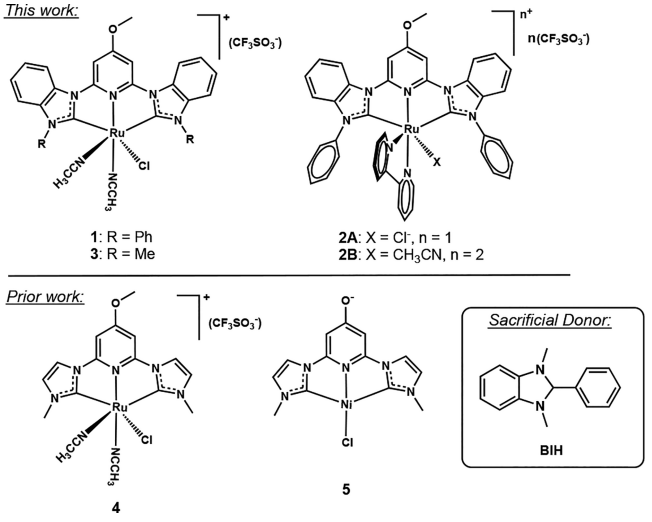

[a]The structure of BIH is also shown.

Received: March 19, 2019

DOI: 10.1021/acs.inorgchem.9b00791
Inorg. Chem. XXXX, XXX, XXX−XXX

Scheme 1. Synthesis of 2A and Conversion to 2B[a]

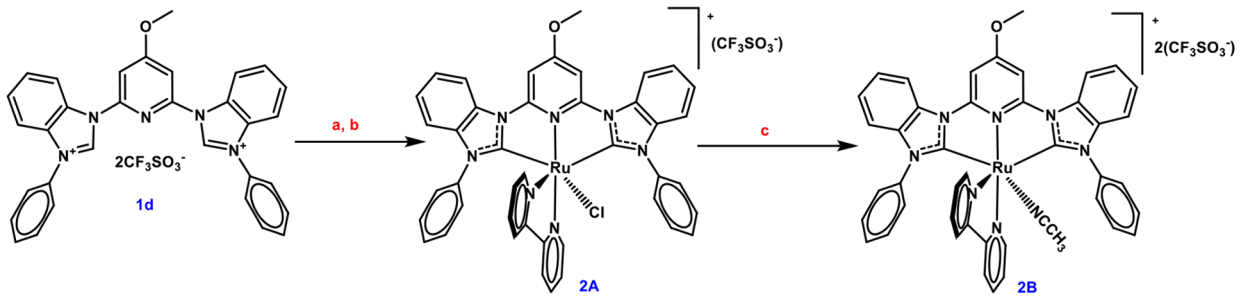

[a]Bis benzimidazolium salt **1d** is used to synthesize complex **2A**, Ru-[{BIm(Me)-py(4-OMe)-BIm(Me)}(bipy)Cl]triflate which is then converted to **2B**, Ru-[{BIm(Me)-py(4-OMe)-BIm(Me)}(bipy)(CH_3CN)]ditriflate. The reagents used are as follows: (a) Ru(bipy)Cl_4, ethylene glycol, saturated aqueous NH_4Cl solution; (b) zinc granules, ethanol; (c) silver trifluoromethanesulfonate, acetonitrile.

catalytic centers.[8−16] We do note that numerous examples of exciting work in the area of visible-light-photosensitized CO_2 reduction catalysis exist with several review articles available;[2−4,17−21] however, this manuscript is written with a focus on self-sensitized reactions using visible light and mononuclear catalysts. The work herein provides an unusual example of a ruthenium-based photocatalyst system with exceptionally high performance for CO_2 reduction.

Our prior report on photosensitized catalysis with **4** showed only trace reactivity in the absence of a photosensitizer during the time period monitored.[5] We hypothesized that an expanded ligand π-system with benzimidazole (in **3**; cf. imidazole in **4**) derived NHC rings could increase the intensity of charge transfer bands, shift light absorption to lower energy, and lead to a photocatalyst. Altering the wingtip substituents of **3** leads to **1** with phenyl groups, which provides a method for increasing steric bulk to limit catalyst−catalyst interactions. Complexes **2A** and **2B** add a 2,2′-bipyridine (bipy) ligand[22−25] to the coordination sphere in place of monodentate ligands in **1**. The bidendate bipy ligand is predicted to increase catalyst stability and accept electron density during a metal-to-ligand charge transfer (MLCT) event more so than the pincer ligand.[9] Given the stronger electron-accepting ability of pyridine versus that of NHC ligands, a redshift is expected to enable broader visible light use. Complexes **2A** and **2B** differ by either the incorporation of a Cl^- or a MeCN ligand, respectively. Given the lability of MeCN ligands, **2B** is predicted to be a faster catalyst due to the easy opening of a free catalytic site.

RESULTS AND DISCUSSION

Synthesis. The synthesis of the pincer ligand of complex **1** starts with a Buchwald−Hartwig coupling between 2,6-dibromo-4-methoxypyridine and N^1-phenylbenzene-1,2-diamine followed by imidazole ring cyclization with triethylorthoformate (Scheme S1).[26−28] Dichloro(*p*-cymene)ruthenium(II) dimer was then used to metalate the ligand to give **1** in 22% overall yield. Attempts to synthesize complex **2A** from **1** through addition of bipy resulted in either a mixture of **2A** and **2B** under thermal conditions or a complex reaction mixture under photolysis conditions. However, complex **2A** was successfully synthesized by modifying a literature procedure and treating (bipy)$Ru^{IV}Cl_4$ with the pincer precursor followed by reduction to Ru^{II} (Scheme 1).[29] Complex **2B** was obtained by salt metathesis upon treating **2A** with silver triflate in acetonitrile (Scheme 1). Complex **3** was synthesized in a manner similar to that described previously for complex **4** (Scheme S3).[5]

Crystal Structures. The crystal structures for complexes **1**, **2A**, **2B**, and **3** are shown in Figure 1. The bond distances and angles are similar to that observed for complex **4** and for other related CNC pincer complexes of ruthenium (Tables S1 and S2, Figure S1). The benzimidazole-derived NHC rings in **1**−**3** feature slightly shorter Ru−C distances versus those of the imidazole-derived NHC in **4** (average = 2.039(6) Å in **1**−**3** versus 2.062(3) Å in **4**, respectively). This is likely due to benzimidazole having an electron-withdrawing effect (cf. imidazole) that enhances the Ru−C π back-bonding.[30] The Ru−N (acetonitrile) distance in **2B** (2.094(6) Å) is elongated relative to that in **1** (average = 2.032(8) Å) and suggests a more labile acetonitrile in **2B**. Notably, the C−O distance of **1**, **2A**, **2B**, and **3** is contracted relative to a C−O single bond (average = 1.346(9) Å versus ∼1.42 Å, respectively), indicating that the methoxy group acts as a π-donor. Furthermore, the pyridine ring is partially dearomatized with long and short C−C distances with the greatest differences in C−C bond lengths being ∼0.03 Å. Thus, the O-donor appears to alter the electronics of the pyridine ring.

UV−Vis Spectroscopy and Electrochemistry. With complexes **1**, **2A**, **2B**, and **3** in hand, the suitability of these complexes for the photocatalytic CO_2 reduction with BIH as a sacrificial electron donor was probed by UV−vis absorption spectroscopy and electrochemical analysis (Figures 2 and S33−S44; Table 1). UV−vis spectra show that the change from imidazole to benzimidazole-derived NHC ligands (in **4** versus **3**) results in a 12 nm redshift in the lowest energy absorption feature. This feature is a broad peak for **3** with a molar absorptivity of 7600 M^{-1} cm^{-1}, which is more intensely absorbing than the low energy transition at 6400 M^{-1} cm^{-1} for **4**. Changing the wingtip methyls (**3**) to phenyls in complex **1** led to very similar electronic spectra in terms of the wavelength absorbed and the molar absorptivity. Replacement of the MeCN ligands of **1** with bipy leads to a longer wavelength absorption (24 nm comparing **2A** to **1**), which may be attributed to a new MLCT event to the bipy ligand. Finally, removal of the chloride and replacement with MeCN to give **2B** from **2A** gave a blueshift; however, **2B** still has significant light absorption in the visible spectrum. Computationally, the assertion that **2A** and **2B** have MLCT events involving the electron transfer to the bipy ligand is supported by the presence of a metal-based HOMO and a bipy-ligand-based LUMO for **2B** (Figure 3). This differs from complex **1** which

DOI: 10.1021/acs.inorgchem.9b00791
Inorg. Chem. XXXX, XXX, XXX−XXX

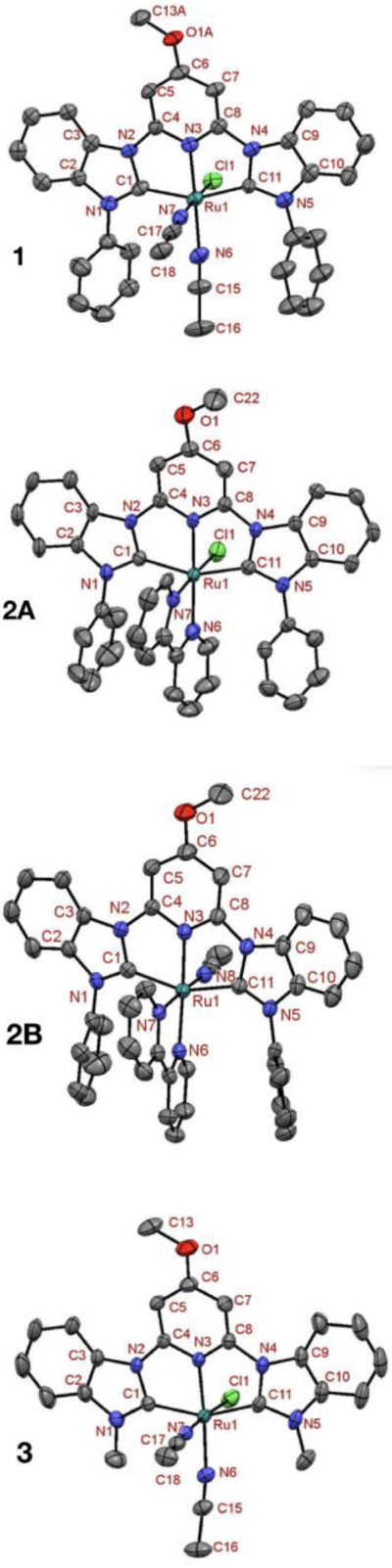

Figure 1. Molecular diagrams of complexes **1**, **2A**, **2B**, and **3** based on crystallographic data with hydrogen atoms and counteranions removed for clarity. Thermal ellipsoids are drawn at the 50% probability level.

shows the LUMO positioned primarily on the pyridine ring of the pincer ligand.

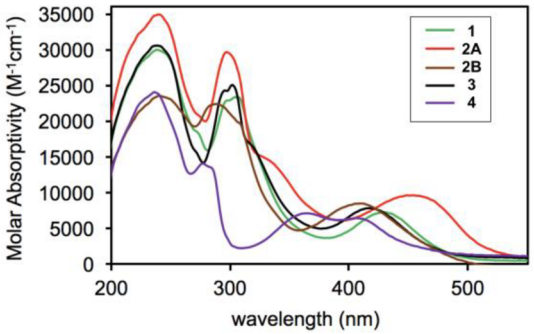

Figure 2. Electronic spectra for each complex in MeCN.

Table 1. Electronic Spectral Features and Electrochemical Redox Potentials for 1−4

cat	λ_{max} (nm)	ε (M^{-1} cm^{-1})	$E_{(S/S-)}$ N_2 (V)[a]	$E_{(S-/S2-)}$ N_2 (V)[b]	$E_{(S/S^-)}$ CO_2 (V)[a,c]	$(i_{cat}/i_p)^2$
1	428	7300	−1.95,[c] −2.16[d]	n/a	−1.80	2.0
2A	452	9800	−1.90,[c] −1.97[d]	−2.15,[c] −2.18[d]	−1.90	2.8
2B	410	8500	−1.85,[c] −1.94[d]	−2.15,[c] −2.16[d]	−1.85	3.7
3	417	7600	−2.15,[c] −2.26[d]	n/a	−2.10	7.8
4	405	6400	−2.30,[c] −2.35[d]	n/a	−2.20	21.4

[a] $E_{(S/S-)}$ is the first reduction potential. [b] $E_{(S-/S2-)}$ is the second reduction potential. [c] From cyclic voltammetry reduction onset. See the Supporting Information for example illustrations of how onset was determined. [d] Differential pulse voltammetry peak potential. These are peak values. See the Supporting Information for voltammograms.

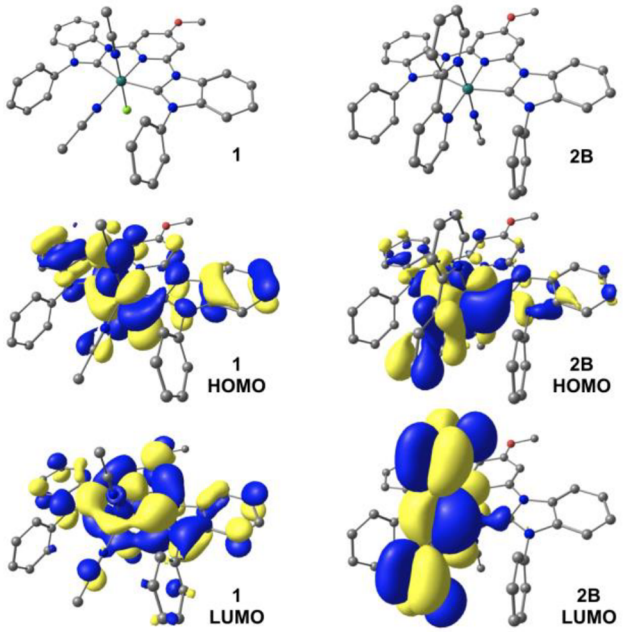

Figure 3. Frontier molecular orbitals for **1** and **2B** calculated at the SMD-PBE0/BS1 level (see the Supporting Information for details).

Electrochemical studies on complexes **1**−**4** were conducted under N_2 and CO_2 atmospheres (Table 1, Figures S35−S44). Via cyclic voltammetry (CV) under N_2 both of the bipy complexes, **2A** and **2B**, show two reductions within the solvent

DOI: 10.1021/acs.inorgchem.9b00791
Inorg. Chem. XXXX, XXX, XXX−XXX

window, while the remaining complexes show just one reduction. All of the reductions were irreversible with complex **1** being the easiest to reduce at −1.95 V vs Fc^+/Fc. Substitution of monodentate ligands (in **1**) with bipy led to a slightly less negative reduction potential for **2A** and **2B** (−1.85 to −1.90 V). Replacement of the phenyl group wingtips with methyl groups led to significantly more negative reduction potentials at −2.15 V for **3** and −2.30 V for **4**. Differential pulse voltammetry (DPV) was also conducted on these complexes under N_2, and the results are in close agreement to the onset potentials observed with CV (Figures S35−S44). Under CO_2, the reduction potential onset does not change dramatically for any of the complexes. A current enhancement was observed for all of the catalysts at the first reduction peak under CO_2 when compared with N_2. The catalytic rate (k_{cat}) for CO_2 reduction is proportional to $(i_{cat}/i_p)^2$ where i_{cat} and i_p are the peak currents observed under CO_2 and nitrogen, respectively.[31,32] Through this estimate (Table 1), electrocatalytic CO_2 reduction rates increase in the following order: **1**< **2A** < **2B**< **3** ≪ **4**.

Photocatalysis. Having found that electrochemical CO_2 reduction occurs in the presence of catalysts **1**-**4**, these catalysts were next tested under photocatalytic reaction conditions. Remarkably, complexes **1**−**4** are catalysts for self-sensitized visible-light-driven CO_2 reduction to CO (Figures 4 and 5, Table 2). All photocatalysis experiments reported herein were performed with TEA and BIH as sacrificial donors in anhydrous acetonitrile with no added PS and quantified via GC (see the Supporting Information for details). In terms of durability, catalyst **2B** was found to be the most durable at 55 TON over a 20 h irradiation period before ceasing CO production. To test for the presence of a heterogeneous catalyst, mercury was added to a photocatalytic reaction with **2B**, and there was no significant difference in catalyst performance (Figure S49).[6] This suggests **2B** is a homogeneous catalyst, although we note that proving homogeneity is challenging.[33−35]

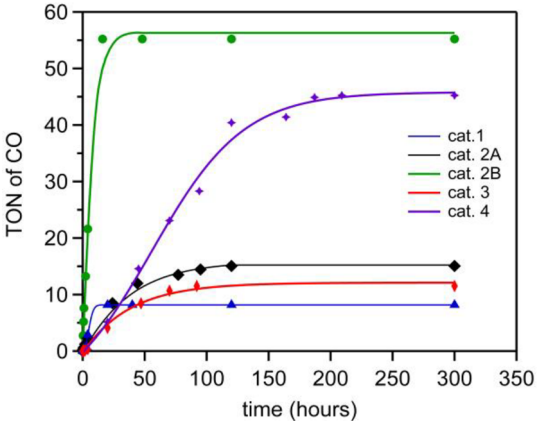

Figure 4. Catalyst TON versus time plot for CO production from **1**−**4**. Reactions are run after vigorous bubbling with CO_2 for 15 min with 0.2 μmol of catalyst and 0.2 mmol of BIH in 2 mL of a 5% TEA/MeCN solution. Solutions are irradiated with a solar simulated spectrum set to 1 sun (150 W Xe lamp, AM 1.5G filter).

The remaining complexes were found to have TON values ranging from 55 to 8 TON in the following order under identical conditions: **2B** > **4** > **2A** > **3** > **1** (Figure 4, Table 2). The high performance from **4** is surprising given our previously reported results.[5] This result can be better understood by analyzing the initial turnover frequency (TOF) values at 20 min which range from 8.3 to 0 h^{-1} (inactive) and decrease in the following order: **2B** > > **2A** > **1** = **3** = **4** (Figure 5, Table 2). Interestingly, this order changes when the maximum TOF values observed are analyzed with **2B** > **1** > **2A** > **4** > **3**. Precatalysts **1**, **3**, and **4** have significant periods of slow catalysis possibly due to either an induction period or not enough product accumulating for detection, with catalysis clearly detectable after 1−20 h (clearly detectable defined as >1 TON). Precatalysts **1** and **3** ultimately reach 8 and 12 TON of CO and are durable for 22 and 95 h, respectively; thus, both perform sluggishly even after activation (Table 2). Precatalyst **4** has the slowest initial rate, but after activation, catalysis continues for 200 h producing the second highest TON value (45) before catalysis ceases. In contrast, rapid initial catalysis is observed for **2A** and **2B**, and Figure 5 shows an expanded view of the early time points from Figure 4. These early data points for the first hour show a constant rate of CO production apparent from a linear fit with an R^2 value of >0.99 and a zero intercept (Figures 4 and 5). No change in slope occurs until catalyst death after several hours for these complexes. Thus, **2A** and **2B** appear to be true catalysts.

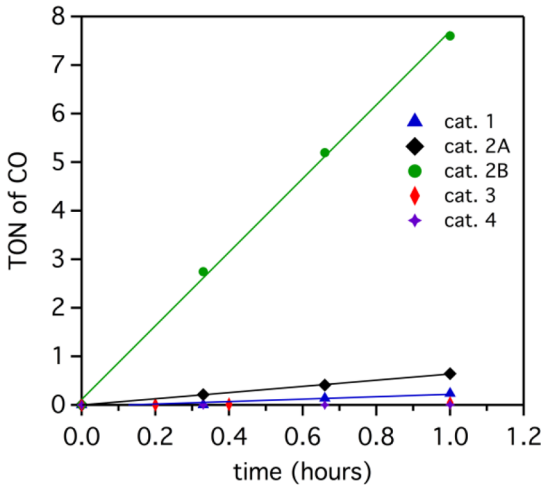

Figure 5. Catalyst TON versus time for the first hour of CO production.

During the photoreaction of **1** and **3**, a white precipitate was observed to form after extended reaction times with CO production. We reasoned this white solid could be accumulation of carbonate from a disproportionation reaction of 2 CO_2 molecules to CO and CO_3^{2-}. Through the use of $^{13}CO_2$, $^{13}CO_3^{2-}$ could be observed in these reactions by ^{13}C NMR (Figure S46). The white solid certainly attenuates the photon flux reaching **1**; thus, photocatalysis experiments were performed without stirring to allow the solids to settle. With this protocol, the TON and TOF values increased significantly from 8 and 1.1 h^{-1} with stirring to 33 and 7.0 h^{-1} without stirring.

As mentioned previously, catalysts **2A** and **2B** have initial TOF values matching the maximum TOF values (Table 2). This suggests that they enter the catalytic cycle by a facile process such as MeCN dissociation in the case of **2B**. Since rapid initial catalysis is observed for these catalysts a pincer or bipy ligand dissociation process is highly unlikely. Catalyst **2B** significantly outperforms **2A** both in terms of durability (55 versus 15 TON) and rate (8.3 versus 0.6 h^{-1} TOF). This

DOI: 10.1021/acs.inorgchem.9b00791
Inorg. Chem. XXXX, XXX, XXX−XXX

Table 2. Comparison of Catalyst Performance Using New Complexes 1−4 and Literature Benchmarks 6−12

entry	cat.	conc.	TON (CO)	TOF (h^{-1}) @20 min	TOF (h^{-1}) max[a]	ϕ_{CO} (%)[b]
1	**1**	0.1 mM	8	0.0	1.1	0.4×10^{-1}
2[c]	**1**	0.1 mM	33	0.0	7.0	9.1×10^{0}
3	**2A**	0.1 mM	15	0.6	0.7	0.2×10^{-1}
4	**2B**	0.1 mM	55	8.3	8.3	2.6×10^{-1}
5[c,d]	**1**	0.1 mM	158	2.0	7.0	19.3×10^{0}
6	**2B**	1.0 nM	33,000	250	250	5.4×10^{-5}
7	**3**	0.1 mM	12	0.0	0.2	0.1×10^{-1}
8	**4**	0.1 mM	45	0.0	0.5	0.2×10^{-1}
9[f]	**6**[e]	0.1 mM	14	11.2	15.9	4.8×10^{-1}
10[f]	**7**[e]	0.1 mM	32	31.6	31.6	10.2×10^{-1}
11[f]	**8**[e]	0.1 mM	3	3.2	3.2	1.0×10^{-1}
12[g]	**8**[e]	0.1 mM	97	96.7	96.7	26.6×10^{-1}
13[h]	**8**[e]	0.5 mM	80[i]	24.1[i]	24.1[i]	
14[h]	**9**[e]	0.1 mM	20[j]	1.5[i]	0.2[i]	
15[h]	**10**[e]	2.0 μM	101	1.4[i]	1.4[i]	
16[h]	**11**[e]	0.9 mM	48		12	
17[h]	**12**[e]	40 μM	160[i]	14.5[h]	14.5	

[a]TOF values were calculated from the fastest reaction rates observed over a 1 h period of photocatalysis. [b]ϕ_{CO} is calculated using a full spectrum solar simulator at 1 sun irradiation intensity, not an isolated wavelength with reduced photon flux as is sometimes reported. ϕ_{CO} is reported as the highest value observed between two time points. [c]Without stirring. [d]Using 1 equiv of bipy added relative to the complex. [e]**6** = $Re(bipy)(CO)_3Br$;[10,11] **7** = $Re(pyNHC\text{-}PhCF_3)(CO)_3Br$;[9,13] **8** = $[Ir(ppy)(terpy)Cl]^+$;[8] **9** = $[Ir(terpy)(bipy)Cl]^{2+}$;[14] **10** = Fe-p-TMA;[12,36] **11** = $Re(bipy)(CO)_3Cl$;[15] **12** = $[Ru(terpy)(pqn)(MeCN)]^{2+}$.[37] See Figure S53 for the catalyst structures. [f]These entries use the benchmark catalysts under the same conditions as entries 1−5. [g]This entry uses the conditions reported in the manuscript with a solar simulated spectrum as the irradiation source. [h]These entries are reported with the highest values observed in the referenced reports of these catalysts. The conditions vary significantly from those in our manuscript in many cases, especially with regard to irradiation wavelengths and filters which can have dramatic effects.[38] [i]Estimated from data in the manuscript. [j]Value is for HCO_2^-.

illustrates that chloride removal greatly enhances self-sensitized catalysis (**2B** versus **2A**). Presumably, the acetonitrile ligand in **2B** is more labile than a chloride and can be more easily displaced during the catalytic cycle. It appears that the bipy coligand is needed for self-sensitized catalysis without an activation period which may be due to a difference in the MLCT state as suggested by the UV−vis absorption data above. Catalyst **1** differs from **2A** in only a bipy ligand substitution for two acetonitrile ligands, and during synthesis, some **2A** and **2B** are observed upon mixing **1** with bipy. Therefore, an experiment was conducted with **1** and added bipy in the reaction mixture without stirring. In this case, a TON value of 158 could be observed, and the catalyst is active from the earliest time points (in contrast to **1** alone). This combination does increase activity with time (from 2.0 to 7.0 h^{-1}), presumably due to a slow displacement of monodentate ligands in **1** for bipy, and ultimately reaches a similar maximal TOF to **2B**. Interestingly addition of more than 1 equiv of bipy resulted in diminished reactivity to 10 TON and a TOF of 0.3 (see Table S6). From the synthetic attempts to make **2A** from **1** and bipy under irradiation, the result is a mixture of complexes with the exact structures of the active catalyst(s) unknown. However, the observed rapid initial catalysis and a significant increase in quantum yield (see discussion below) suggests that the species formed is the active catalyst and that a discrete photosensitizer is likely not present. In all cases, after irradiation the photocatalytic activity is found to stop after 150 h, and in the case of **2B**, catalytic activity ceases abruptly at 16 h even though ample BIH, TEA, and CO_2 remain (see Figure S51 for an NMR of a completed reaction with **2B** showing BIH remaining).

Quantum Yields for CO Production. The quantum yields of these reactions were estimated during the maximum TOF period within at least a 20 min time period via the equation: ϕ_{CO} = [(number of CO molecules × 2)/(number of incident photons)] × 100%, where ϕ_{CO} is the quantum yield for CO production, the number of incident photons is taken as the total number of photons striking the reaction vessel, and a factor of 2 is used to account for the two electrons needed to reduce CO_2 to CO.[39] Using this method, catalyst **2B** shows approximately an order of magnitude higher ϕ_{CO} than that of the remaining complexes, 0.26% versus 0.04−0.01%. The more efficient use of photons by **2B** relative to that of the other complexes highlights the importance of each catalyst structural change from **4** to **2B** with the exchange of the chloride atom for a more labile MeCN ligand being critical (0.02% ϕ_{CO} for **2A** versus 0.26% ϕ_{CO} for **2B**). Interestingly, a high quantum yield of 19.3% is observed for the reaction employing **1** with 1 equiv of added bipy. Importantly, quantum yields in excess of $\sim 1 \times 10^{-2}$ are often indicative of mononuclear photocatalysts at this concentration since PS based systems commonly show lower quantum yields.[39]

Comparison to Literature Catalysts. Under identical conditions, **2B** was found to be a more durable catalyst than the high-performance literature benchmarks $Re(bipy)(CO)_3Br$ (**6**), $Re(pyNHC\text{-}PhCF_3)(CO)_3Br$ (**7**), and $[Ir(ppy)(terpy)Cl]^+$ (**8**) when tested in our laboratory (Table 2, entries 3, 7−9). A near doubling of TON values is observed compared to the next highest performing catalysts tested with **2B** at 55 TON versus 32 TON for **7**. The TOF values were found to be lower for **2B** than for rhenium-based complexes **6** and **7** (8.3 versus 11.2 and 31.6, respectively). ϕ_{CO} measurements show a similar trend when **2B**, **6**, and **7** are compared with values of, respectively, 2.6×10^{-1}, 4.8×10^{-1}, and 10.2×10^{-1} observed. Iridium complex **8** was found to perform substantially lower under identical conditions in terms of TON, TOF, and ϕ_{CO}. The conditions employed in this manuscript differ in SD choice with **2B** using BIH/TEA and **8** using triethanol amine

DOI: 10.1021/acs.inorgchem.9b00791
Inorg. Chem. XXXX, XXX, XXX−XXX

(TEOA) in the original report. Holding all conditions constant and replacing the BIH/TEA SD with TEOA, complex **8** is observed to regain a high performance similar to that reported in literature with 97 TON and a TOF of 97 h^{-1}. This observation serves to highlight that conditions have a very large impact on catalyst performance;[7] thus, direct comparisons of catalyst structure with performance are best made under identical conditions, as in Table 2 (entries 1−11).

However, an expanded comparison to catalysts under different conditions does have merit in that practically a system that maximizes TON, TOF, and ϕ_{CO} is desired. Thus, a comparison to literature observed values is shown in Table 2, entries 13−17, which are under different conditions. The comparison in Table 2 for the complexes **6**−**12** has been limited to the basic parent homogeneous complexes for mononuclear catalysts and to only photocatalysts using visible light to avoid an excessive number of entries. However, we note that many interesting additional examples exist with mononuclear, visible-light-driven, homogeneous photocatalysts (see reviews[2,20,21,40] with ligand derivatives demonstrating TON values of up to 530 at 0.5 mM are obtainable).[38]

When comparing additional catalysts under varying conditions, one of the most important parameters to assess is concentration since this has been observed in several instances to have a dramatic effect on TON, TOF, and ϕ_{CO} in literature and with **2B** as discussed below.[41,42] As reported in the literature,[8] **8** at 0.5 mM shows estimated TON and TOF values of 80 and 24.1 h^{-1} which are higher than the values for **2B** at 0.1 mM. Iridium complex **9** is a structural analogue of **8** with a different charge (2+) and is reported to give 20 turnovers of formate and only 2 turnovers of CO at the same concentration as our studies with **2B**.[14]

Recently, Fe-porphyrin complex **10** has gained significant attention as a photocatalyst with TON and TOF values of 101 and 1.4 h^{-1} reported at 2.0 μM concentration.[12,36] The TON value is higher than that we observe with **2B**, although we note that **2B** has a considerably higher TOF and that the study with **10** was done at significantly lower concentration. The original report on the first visible-light-driven mononuclear homogeneous photocatalyst (**11**), which is now a ubiquitous benchmarking standard in the literature, was done at a similar concentration and shows slightly fewer TONs than **2B** but with a slightly higher TOF than **2B**.[15] Very recently after our work was submitted, $[Ru(terpy)(pqn)(MeCN)]^{2+}$ at 40 μM was shown to self-sensitize CO_2 reduction producing 160 TON of CO with BIH as the sacrificial donor in DMA/H_2O solvent, which appears to be the first report of a mononuclear, visible-light-driven, homogeneous Ru CO_2 reduction catalyst.[37]

Effect of Catalyst Concentration on Photocatalysis. The above comparisons to literature have several variables changed, and concentration is a critical variable when analyzing homogeneous photocatalytic reactions. A reduction in catalyst concentration can often significantly increase catalyst durability by reducing catalyst−catalyst interactions and is potentially a good indicator of how a catalyst may perform when immobilized.[41,43] Additionally, low concentration experiments also allow probing of mechanistic pathways. Bimolecular mechanistic pathways are known in which one complex acts as a photosensitizer and the second as a catalyst.[44,45] This pathway access is reduced at very low concentration as we have previously shown.[42] Since the two highest TON values in literature were reported at much lower concentrations than our original studies with **2B**, an experiment on the effects of diminished concentration on the performance of **2B** was conducted. Accordingly, the catalyst concentration was dramatically reduced to 1 nM to analyze the lowest concentration anticipated to provide significant CO amounts needed for accurate detection. For **2B**, we observe 33 000 TON (TOF = 250 h^{-1}) at 1 nM concentration (Figure S48). The reason for this significant increase in TON and TOF at low concentration can be explained at least in part by an increased number of photons available throughout the solution. At higher concentrations, a significant loss in transmission is evident before and during the reaction with as little as 10% transmittance at ∼425 nm (Figure S54). This indicates that at 0.1 mM photons are not in large excess throughout the reaction, whereas at 1 nM transmittance is measured at >95% during the entire reaction time. With greater than 95% of the photons striking the vessel passing though unabsorbed, a lower ϕ_{CO} value is expected. Notably, the ϕ_{CO} value diminished dramatically (5.4×10^{-5} versus 2.5×10^{-1}) as is expected with a lower amount of chromophore to absorb photons.

Recently, low concentration studies are appearing more commonly in literature and provide a method to demonstrate catalyst performance with photons in large excess and catalyst molecules isolated from one another by solvent. For the case of a practical system where SDs are eliminated and CO_2 reduction catalysts are coupled with oxidative catalysts, a promising direction is to use surface-bound molecular catalysts in photoelectrochemical cells.[46,47] In literature reports of such systems, catalysts are immobilized, and TON values show dramatic increases when the surface bound system is compared with high-concentration homogeneous studies.[48−54] Low-concentration homogeneous studies could likely become a key parameter in catalyst selection for immobilization. To the best of our knowledge, the TON and TOF values observed herein are record-setting for a mononuclear photocatalyst driving CO_2 reduction. The expansion of comparison to other conditions shows that catalyst **2B** has comparable performance to the best self-sensitized catalysts at high concentration (0.1 mM) and exceptional performance at low concentration (1.0 nM). This indicates that **2B** is unusually robust and high-performing among mononuclear visible-light-driven systems, and **2B** serves as the second example using ruthenium and visible light to reduce CO_2.

Comparing Photocatalysis to Other Methods of CO_2 Reduction. In general, when comparing these reactions to other CO_2 reduction methods, homogeneous photocatalytic CO_2 reduction proceeds at significantly slower reaction rates than those commonly observed for electrocatalysis and thermal-based approaches to CO_2 reduction. However, we stress that studies within the homogeneous photocatalysis field are analyzing half-reactions with sacrificial electron donors and are not predictive for rates in future large-scale practical applications which will likely exclude reagents such as BIH, TEA, and MeCN due to cost constraints. Rather, practical applications will likely be restricted to water as both the solvent and the source of electrons. Importantly, the choice of electron donor can have a profound influence on rates and even product distributions obtained from CO_2 reduction.[7] Significant caution is warranted in comparing reaction rates between different systems where the rate in question could be more dependent on the sacrificial donor rather than on CO_2 bond cleavage. Nonetheless, studies of these half-reactions with sacrificial donors allow for the rapid analysis of catalyst

DOI: 10.1021/acs.inorgchem.9b00791
Inorg. Chem. XXXX, XXX, XXX−XXX

durability. Several examples are discussed above which were heterogenized onto semiconductors to produce faster reaction rates and increased durability. There is certainly appeal in studying homogeneous catalysis as it allows for rapid access to simplified systems where modifications lead to predictable changes for trend establishment in many cases. Since immobilization onto an electrode surface results in significantly higher durability in many cases, low-concentration studies limiting catalyst−catalyst interactions with excess photons present are desirable to get a reasonable prediction in a simplified system as to how the catalyst will behave in a more practical setting.

CONCLUSION

In conclusion, four Ru-complexes were synthesized, characterized, and studied in the photocatalytic reduction of CO_2 reaction. Through structure−function analysis, it was found that phenyl wingtip pincer complexes with benzimidazoles were more active in this reaction than the methyl wingtip imidazole analogues. The incorporation of a bipy ligand into the catalyst design proved critical to observing rapid initial catalysis. Incorporating all of these design elements into $[(CNC)Ru(bipy)CH_3CN)](OTf)_2$ (**2B**) led to one of the fastest and most durable photocatalysts known. Catalyst **2B** is among the most active catalysts in the literature for self-sensitized CO_2 reduction, and further mechanistic studies and incorporation into photoelectrochemical cells present an exciting opportunity for harnessing solar energy to produce solar fuels.

ASSOCIATED CONTENT

Supporting Information

The Supporting Information is available free of charge on the ACS Publications website at DOI: 10.1021/acs.inorgchem.9b00791.

Experimental details on synthesis and characterization, single crystal X-ray diffraction, photocatalysis, and computations (PDF)

Crystallographic information (XYZ)

Accession Codes

CCDC 1879281−1879284 contain the supplementary crystallographic data for this paper. These data can be obtained free of charge via www.ccdc.cam.ac.uk/data_request/cif, or by emailing data_request@ccdc.cam.ac.uk, or by contacting The Cambridge Crystallographic Data Centre, 12 Union Road, Cambridge CB2 1EZ, UK; fax: +44 1223 336033.

AUTHOR INFORMATION

Corresponding Authors

*E-mail: ewebster@chemistry.msstate.edu (C.E.W.)
*E-mail: delcamp@olemiss.edu (J.H.D.).
*E-mail: etpapish@ua.edu (E.T.P.).

ORCID

Roberta R. Rodrigues: 0000-0003-2930-2451
Fengrui Qu: 0000-0002-9975-2573
Chance M. Boudreaux: 0000-0003-1322-9878
Charles Edwin Webster: 0000-0002-6917-2957
Jared H. Delcamp: 0000-0001-5313-4078
Elizabeth T. Papish: 0000-0002-7937-8019

Author Contributions

#S.D. and R.R.R. contributed equally to this work.

Notes

The authors declare the following competing financial interest(s): E.T.P. and J.H.D. have filed a patent application related to this chemistry.

ACKNOWLEDGMENTS

We thank the NSF (awards CHE-1800281, 1800214, and 1800201) for funding this research. Preliminary data was also obtained with NSF OIA-1539035 support. S.D. thanks the University of Alabama's Graduate Council Fellowship (GCF), and C.M.B. is grateful for a GAANN fellowship (Department of Education P200A150329) for partial support.

REFERENCES

(1) Robert, M. Running the Clock: CO_2 Catalysis in the Age of Anthropocene. *ACS Energy Lett.* **2016**, *1*, 281−282.

(2) Hammer, N. I.; Sutton, S.; Delcamp, J. H.; Graham, J. D. *Handbook of Climate Change Mitigation and Adaptation 2017*; Chen, W. Y., Suzuki, T., Lackner, M., Eds.; Springer, DOI: 10.1007/978-3-319-14409-2_46.

(3) White, J. L.; Baruch, M. F.; Pander, J. E.; Hu, Y.; Fortmeyer, I. C.; Park, J. E.; Zhang, T.; Liao, K.; Gu, J.; Yan, Y.; Shaw, T. W.; Abelev, E.; Bocarsly, A. B. Light-Driven Heterogeneous Reduction of Carbon Dioxide: Photocatalysts and Photoelectrodes. *Chem. Rev.* **2015**, *115*, 12888−12935.

(4) Liu, X.; Inagaki, S.; Gong, J. Heterogeneous Molecular Systems for Photocatalytic CO_2 Reduction with Water Oxidation. *Angew. Chem., Int. Ed.* **2016**, *55*, 14924−14950.

(5) Boudreaux, C. M.; Liyanage, N. P.; Shirley, H.; Siek, S.; Gerlach, D. L.; Qu, F.; Delcamp, J. H.; Papish, E. T. Ruthenium(II) complexes of pyridinol and N-heterocyclic carbene derived pincers as robust catalysts for selective carbon dioxide reduction. *Chem. Commun.* **2017**, *53*, 11217−11220.

(6) Burks, D. B.; Davis, S.; Lamb, R. W.; Liu, X.; Rodrigues, R. R.; Liyanage, N. P.; Sun, Y.; Webster, C. E.; Delcamp, J. H.; Papish, E. T. Nickel(II) pincer complexes demonstrate that the remote substituent controls catalytic carbon dioxide reduction. *Chem. Commun.* **2018**, *54*, 3819−3822.

(7) Rodrigues, R. R.; Boudreaux, C. M.; Papish, E. T.; Delcamp, J. H. Photocatalytic Reduction of CO_2 to CO and Formate: Do Reaction Conditions or Ruthenium Catalysts Control Product Selectivity? *ACS Appl. Energy Mater.* **2019**, *2*, 37−46.

(8) Sato, S.; Morikawa, T.; Kajino, T.; Ishitani, O. A Highly Efficient Mononuclear Iridium Complex Photocatalyst for CO_2 Reduction under Visible Light. *Angew. Chem., Int. Ed.* **2013**, *52*, 988−992.

(9) Huckaba, A. J.; Sharpe, E. A.; Delcamp, J. H. Photocatalytic Reduction of CO_2 with Re-Pyridyl-NHCs. *Inorg. Chem.* **2016**, *55*, 682−690.

(10) Hori, H.; Johnson, F. P. A.; Koike, K.; Ishitani, O.; Ibusuki, T. Efficient photocatalytic CO_2 reduction using $[Re(bpy)(CO)_3\{P(OEt)_3\}]+$. *J. Photochem. Photobiol., A* **1996**, *96*, 171−174.

(11) Hawecker, J.; Lehn, J.-M.; Ziessel, R. Photochemical and Electrochemical Reduction of Carbon Dioxide to Carbon Monoxide Mediated by (2,2′-Bipyridine)tricarbonylchlororhenium(I) and Related Complexes as Homogeneous Catalysts. *Helv. Chim. Acta* **1986**, *69*, 1990−2012.

(12) Rao, H.; Bonin, J.; Robert, M. Non-sensitized selective photochemical reduction of CO_2 to CO under visible light with an iron molecular catalyst. *Chem. Commun.* **2017**, *53*, 2830−2833.

(13) Carpenter, C.; Brogdon, P.; McNamara, L.; Tschumper, G.; Hammer, N.; Delcamp, J. A Robust Pyridyl-NHC-Ligated Rhenium Photocatalyst for CO_2 Reduction in the Presence of Water and Oxygen. *Inorganics* **2018**, *6*, 22.

(14) Sato, S.; Morikawa, T. [Ir(tpy)(bpy)Cl] as a Photocatalyst for CO2 Reduction under Visible-Light Irradiation. *ChemPhotoChem* **2018**, *2*, 207.

DOI: 10.1021/acs.inorgchem.9b00791
Inorg. Chem. XXXX, XXX, XXX−XXX

(15) Hawecker, J.; Lehn, J.-M.; Ziessel, R. Efficient photochemical reduction of CO_2 to CO by visible light irradiation of systems containing $Re(bipy)(CO)_3X$ or $[Ru(bipy)_3]^{2+}$-Co^{2+} combinations as homogeneous catalysts. *J. Chem. Soc., Chem. Commun.* **1983**, 536−538.
(16) Morris, A. J.; Meyer, G. J.; Fujita, E. Molecular Approaches to the Photocatalytic Reduction of Carbon Dioxide for Solar Fuels. *Acc. Chem. Res.* **2009**, *42*, 1983−1994.
(17) Elgrishi, N.; Chambers, M. B.; Wang, X.; Fontecave, M. Molecular polypyridine-based metal complexes as catalysts for the reduction of CO2. *Chem. Soc. Rev.* **2017**, *46*, 761−796.
(18) Reithmeier, R.; Bruckmeier, C.; Rieger, B. Conversion of CO_2 via Visible Light Promoted Homogeneous Redox Catalysis. *Catalysts* **2012**, *2*, 544.
(19) Sahara, G.; Ishitani, O. Efficient Photocatalysts for CO_2 Reduction. *Inorg. Chem.* **2015**, *54*, 5096−5104.
(20) Takeda, H.; Cometto, C.; Ishitani, O.; Robert, M. Electrons, Photons, Protons and Earth-Abundant Metal Complexes for Molecular Catalysis of CO_2 Reduction. *ACS Catal.* **2017**, *7*, 70−88.
(21) Kuramochi, Y.; Ishitani, O.; Ishida, H. Reaction mechanisms of catalytic photochemical CO_2 reduction using Re(I) and Ru(II) complexes. *Coord. Chem. Rev.* **2018**, *373*, 333−356.
(22) Guisado-Barrios, G.; Bouffard, J.; Donnadieu, B.; Bertrand, G. Bis(1,2,3-triazol-5-ylidenes) (i-bitz) as Stable 1,4-Bidentate Ligands Based on Mesoionic Carbenes (MICs). *Organometallics* **2011**, *30*, 6017−6021.
(23) Guisado-Barrios, G.; Soleilhavoup, M.; Bertrand, G. 1H-1,2,3-Triazol-5-ylidenes: Readily Available Mesoionic Carbenes. *Acc. Chem. Res.* **2018**, *51*, 3236−3244.
(24) Gierz, V.; Maichle-Mössmer, C.; Kunz, D. 1,10-Phenanthroline Analogue Pyridazine-Based N-Heterocyclic Carbene Ligands. *Organometallics* **2012**, *31*, 739−747.
(25) Kunz, D.; Flaig, K. S. The coordinative flexibility of rigid phenanthroline-analogous di(NHC)-ligands. *Coord. Chem. Rev.* **2018**, *377*, 73−85.
(26) Tokmic, K.; Markus, C. R.; Zhu, L.; Fout, A. R. Well-Defined Cobalt(I) Dihydrogen Catalyst: Experimental Evidence for a Co(I)/Co(III) Redox Process in Olefin Hydrogenation. *J. Am. Chem. Soc.* **2016**, *138*, 11907−11913.
(27) Kim, D.; Le, L.; Drance, M. J.; Jensen, K. H.; Bogdanovski, K.; Cervarich, T. N.; Barnard, M. G.; Pudalov, N. J.; Knapp, S. M. M.; Chianese, A. R. Ester Hydrogenation Catalyzed by CNN-Pincer Complexes of Ruthenium. *Organometallics* **2016**, *35*, 982−989.
(28) Chianese, A. R.; Mo, A.; Lampland, N. L.; Swartz, R. L.; Bremer, P. T. Iridium Complexes of CCC-Pincer N-Heterocyclic Carbene Ligands: Synthesis and Catalytic C-H Functionalization. *Organometallics* **2010**, *29*, 3019−3026.
(29) Chung, L.-H.; Cho, K.-S.; England, J.; Chan, S.-C.; Wieghardt, K.; Wong, C.-Y. Ruthenium(II) and Osmium(II) Complexes Bearing Bipyridine and the N-Heterocyclic Carbene-Based C-N-C Pincer Ligand: An Experimental and Density Functional Theory Study. *Inorg. Chem.* **2013**, *52*, 9885−9896.
(30) Gradert, C.; Krahmer, J.; Sönnichsen, F. D.; Näther, C.; Tuczek, F. Molybdenum(0)-carbonyl complexes supported by mixed benzimidazol-2-ylidene/phosphine ligands: Influence of benzannulation on the donor properties of the NHC groups. *J. Organomet. Chem.* **2014**, *770*, 61−68.
(31) Coggins, M. K.; Zhang, M.-T.; Chen, Z.; Song, N.; Meyer, T. J. Single-Site Copper(II) Water Oxidation Electrocatalysis: Rate Enhancements with HPO_4^{2-} as a Proton Acceptor at pH 8. *Angew. Chem., Int. Ed.* **2014**, *53*, 12226−12230.
(32) Zhang, T.; Wang, C.; Liu, S.; Wang, J.-L.; Lin, W. A Biomimetic Copper Water Oxidation Catalyst with Low Overpotential. *J. Am. Chem. Soc.* **2014**, *136*, 273−281.
(33) Widegren, J. A.; Bennett, M. A.; Finke, R. G. Is It Homogeneous or Heterogeneous Catalysis? Identification of Bulk Ruthenium Metal as the True Catalyst in Benzene Hydrogenations Starting with the Monometallic Precursor, $Ru(II)(\eta^6\text{-}C_6Me_6)(OAc)_2$, Plus Kinetic Characterization of the Heterogeneous Nucleation, Then Autocatalytic Surface-Growth Mechanism of Metal Film Formation. *J. Am. Chem. Soc.* **2003**, *125*, 10301−10310.
(34) Crabtree, R. H. Resolving Heterogeneity Problems and Impurity Artifacts in Operationally Homogeneous Transition Metal Catalysts. *Chem. Rev.* **2012**, *112*, 1536−1554.
(35) Artero, V.; Fontecave, M. Solar fuels generation and molecular systems: is it homogeneous or heterogeneous catalysis? *Chem. Soc. Rev.* **2013**, *42*, 2338−2356.
(36) Rao, H.; Schmidt, L. C.; Bonin, J.; Robert, M. Visible-light-driven methane formation from CO_2 with a molecular iron catalyst. *Nature* **2017**, *548*, 74.
(37) Lee, S. K.; Kondo, M.; Okamura, M.; Enomoto, T.; Nakamura, G.; Masaoka, S. Function-Integrated Ru Catalyst for Photochemical CO_2 Reduction. *J. Am. Chem. Soc.* **2018**, *140*, 16899−16903.
(38) Genoni, A.; Chirdon, D. N.; Boniolo, M.; Sartorel, A.; Bernhard, S.; Bonchio, M. Tuning Iridium Photocatalysts and Light Irradiation for Enhanced CO_2 Reduction. *ACS Catal.* **2017**, *7*, 154−160.
(39) Bonin, J.; Robert, M.; Routier, M. Selective and Efficient Photocatalytic CO_2 Reduction to CO Using Visible Light and an Iron-Based Homogeneous Catalyst. *J. Am. Chem. Soc.* **2014**, *136*, 16768−16771.
(40) Takeda, H.; Koike, K.; Morimoto, T.; Inumaru, H.; Ishitani, O. Photochemistry and photocatalysis of rhenium(I) diimine complexes. *Adv. Inorg. Chem.* **2011**, *63*, 137−186.
(41) Thoi, V. S.; Kornienko, N.; Margarit, C. G.; Yang, P.; Chang, C. J. Visible-Light Photoredox Catalysis: Selective Reduction of Carbon Dioxide to Carbon Monoxide by a Nickel N-Heterocyclic Carbene-Isoquinoline Complex. *J. Am. Chem. Soc.* **2013**, *135*, 14413−14424.
(42) Liyanage, N. P.; Yang, W.; Guertin, S.; Sinha Roy, S.; Carpenter, C. A.; Adams, R. E.; Schmehl, R. H.; Delcamp, J. H.; Jurss, J. W. Photochemical CO_2 reduction with mononuclear and dinuclear rhenium catalysts bearing a pendant anthracene chromophore. *Chem. Commun.* **2019**, *55*, 993−996.
(43) Guo, Z.; Yu, F.; Yang, Y.; Leung, C.-F.; Ng, S.-M.; Ko, C.-C.; Cometto, C.; Lau, T.-C.; Robert, M. Photocatalytic Conversion of CO_2 to CO by a Copper(II) Quaterpyridine Complex. *ChemSusChem* **2017**, *10*, 4009−4013.
(44) Takeda, H.; Koike, K.; Inoue, H.; Ishitani, O. Development of an Efficient Photocatalytic System for CO_2 Reduction Using Rhenium(I) Complexes Based on Mechanistic Studies. *J. Am. Chem. Soc.* **2008**, *130*, 2023−2031.
(45) Kou, Y.; Nabetani, Y.; Masui, D.; Shimada, T.; Takagi, S.; Tachibana, H.; Inoue, H. Direct Detection of Key Reaction Intermediates in Photochemical CO_2 Reduction Sensitized by a Rhenium Bipyridine Complex. *J. Am. Chem. Soc.* **2014**, *136*, 6021−6030.
(46) Sekizawa, K.; Maeda, K.; Domen, K.; Koike, K.; Ishitani, O. Artificial Z-Scheme Constructed with a Supramolecular Metal Complex and Semiconductor for the Photocatalytic Reduction of CO_2. *J. Am. Chem. Soc.* **2013**, *135*, 4596−4599.
(47) Sahara, G.; Kumagai, H.; Maeda, K.; Kaeffer, N.; Artero, V.; Higashi, M.; Abe, R.; Ishitani, O. Photoelectrochemical Reduction of CO_2 Coupled to Water Oxidation Using a Photocathode With a Ru(II)-Re(I) Complex Photocatalyst and a CoOx/TaON Photoanode. *J. Am. Chem. Soc.* **2016**, *138*, 14152−14158.
(48) Ha, E. G.; Chang, J. A.; Byun, S. M.; Pac, C.; Jang, D. M.; Park, J.; Kang, S. O. High-turnover visible-light photoreduction of CO_2 by a Re(I) complex stabilized on dye-sensitized TiO_2. *Chem. Commun.* **2014**, *50*, 4462−4.
(49) Won, D. I.; Lee, J. S.; Ji, J. M.; Jung, W. J.; Son, H. J.; Pac, C.; Kang, S. O. Highly Robust Hybrid Photocatalyst for Carbon Dioxide Reduction: Tuning and Optimization of Catalytic Activities of Dye/TiO_2/Re(I) Organic-Inorganic Ternary Systems. *J. Am. Chem. Soc.* **2015**, *137*, 13679−90.
(50) Windle, C. D.; Pastor, E.; Reynal, A.; Whitwood, A. C.; Vaynzof, Y.; Durrant, J. R.; Perutz, R. N.; Reisner, E. Improving the Photocatalytic Reduction of CO_2 to CO through Immobilisation of a Molecular Re Catalyst on TiO_2. *Chem. - Eur. J.* **2015**, *21*, 3746−3754.

DOI: 10.1021/acs.inorgchem.9b00791
Inorg. Chem. XXXX, XXX, XXX−XXX

(51) Kuriki, R.; Matsunaga, H.; Nakashima, T.; Wada, K.; Yamakata, A.; Ishitani, O.; Maeda, K. Nature-Inspired, Highly Durable CO_2 Reduction System Consisting of a Binuclear Ruthenium(II) Complex and an Organic Semiconductor Using Visible Light. *J. Am. Chem. Soc.* **2016**, *138*, 5159−70.
(52) Brennaman, M. K.; Dillon, R. J.; Alibabaei, L.; Gish, M. K.; Dares, C. J.; Ashford, D. L.; House, R. L.; Meyer, G. J.; Papanikolas, J. M.; Meyer, T. J. Finding the Way to Solar Fuels with Dye-Sensitized Photoelectrosynthesis Cells. *J. Am. Chem. Soc.* **2016**, *138*, 13085−13102.
(53) Sahara, G.; Abe, R.; Higashi, M.; Morikawa, T.; Maeda, K.; Ueda, Y.; Ishitani, O. Photoelectrochemical CO_2 reduction using a Ru(II)-Re(I) multinuclear metal complex on a p-type semiconducting NiO electrode. *Chem. Commun.* **2015**, *51*, 10722−5.
(54) Woo, S.-J.; Choi, S.; Kim, S.-Y.; Kim, P. S.; Jo, J. H.; Kim, C. H.; Son, H.-J.; Pac, C.; Kang, S. O. Highly Selective and Durable Photochemical CO_2 Reduction by Molecular Mn(I) Catalyst Fixed on a Particular Dye-Sensitized TiO_2 Platform. *ACS Catal.* **2019**, *9*, 2580−2593.

DOI: 10.1021/acs.inorgchem.9b00791
Inorg. Chem. XXXX, XXX, XXX−XXX